Research Article | Vol. 32, No. 16 / 29 Jul 2024 / Optics Express 27303

Optics EXPRESS

Three-dimensional reconstruction method for layered structures based on a frequency modulated continuous wave terahertz radar

KAILIANG XUE,[1] WENNA ZHANG,[1] JIALIN SONG,[1] ZHAOBA WANG,[1,2] YONG JIN,[1,2] ASOKE K. NANDI,[3] AND YOUXING CHEN[1,2,*]

[1] *School of Information and Communication Engineering, North University of China, Taiyuan 030051, China*
[2] *National Key Laboratory for Electronic Measurement Technology, North University of China, Taiyuan 030051, China*
[3] *Department of Electronic and Computer Engineering, Brunel University London, London UB8 3 PH, United Kingdom*
[*] *chenyouxing@nuc.edu.cn*

Abstract: The feasibility of employing a continuous-wave terahertz detection system for non-contact and non-destructive testing (NDT) in multi-layered bonding structures is assessed in this study. The paper introduces the detection principle of terahertz frequency modulated continuous wave (FMCW) radar and outlines the two-dimensional (2D) scanning platform, which integrates optical lenses, three linear actuators, a control platform, and data acquisition units. Experimental results on two types of insulation with prefabricated defects demonstrate the capability of terahertz waves for transparent inspection imaging. These results confirm the viability of terahertz FMCW detection technology as an advanced NDT tool for multi-layered bonding structures. However, the inherent limitations of terahertz wavelength and hardware systems pose challenges in discriminating reflection peaks on upper and lower surfaces. To address this issue, a local adaptive empirical wavelet coefficient modal decomposition (LAEWCMD) method is proposed to enhance the longitudinal discrimination ability of terahertz detection. The proposed method involves segmenting the 2D terahertz detection image into regions to differentiate between defective and non-defective areas. Continuous wavelet transforms (CWT) are then applied to the range signals of each region to derive continuous wavelet coefficients (CWCs). Subsequently, empirical mode decomposition (EMD) is performed on the CWCs to decompose them into intrinsic mode functions (IMFs) and residual signals. The 1st IMF is utilized for three-dimensional (3D) reconstruction, and the regions are fused to generate the final output. The effectiveness of the proposed method is validated on aircraft thermal protection structures (TPS), achieving high-precision 3D reconstruction. This offers a novel approach for the application of terahertz computed tomography imaging and NDT.

1. Introduction

Layered structures are widely used in military and civilian products such as aircraft thermal protection structures (TPS) [1–2], coatings inside solid rocket engines [3], and corrosion protection layers for gas and oil pipelines [4]. The adhesive quality of each layered interface is crucial for the safe service of the components. Taking aircraft TPS as an example, it is made of ceramic matrix composites (CMC), insulating felt, and protected structures sequentially bonded by adhesives. Due to the influence of production processes and service environments, debonding and delamination are occurred easily between TPS and aircraft shell, which will greatly affect the thermal insulation performance, and lay a major hidden danger for the safety of the flight

#528258
Journal © 2024

https://doi.org/10.1364/OE.528258
Received 30 Apr 2024; revised 27 Jun 2024; accepted 7 Jul 2024; published 15 Jul 2024

Optics EXPRESS

of the aircraft [1,2,5]. Therefore, the use of non-destructive testing (NDT) methods to assess the bonding condition is essential. With the advancement of terahertz radiation and detection technologies, terahertz NDT has gradually become a research hot spot [6–8].

Terahertz waves, with frequencies ranging from 0.1 THz to 10 THz, occupy a unique position within the electromagnetic spectrum, nestled between the realms of millimeter waves and infrared radiation. This positioning grants terahertz waves a dual nature, embodying characteristics of both electronics and photonics [9–11]. On the one hand, their intriguing properties make them particularly adept at interacting with non-polar materials (such as ceramics, rubber, resin and other composite materials), offering notable penetration capabilities and interface reflectivity. Consequently, terahertz waves surpass traditional NDT methods in their ability to detect and pinpoint internal material defects, heralding a new era of contactless inspection [12]. On the other hand, owing to their modest photon energy levels, terahertz waves pose minimal risk of harm to the samples under scrutiny and the human body. As terahertz technology continues to advance and mature, its applications have proliferated across a diverse array of fields such as composite material detection [13–15], security screening [16], mail inspection [17], cultural heritage conservation [18], and biomedical imaging [19] and other aspects. More specifically, terahertz NDT makes up for the shortcomings of traditional NDT methods to a certain extent, and provides a new solution for health monitoring of composite materials. Typical representative devices include Time-domain Spectroscopy (TDS) and Frequency Modulated Continuous Wave (FMCW) imaging system.

The unique potential of FMCW sensing stems from its inherent advantages such as high integration and compactness, robustness of the measurement process, and lower cost. The terahertz FMCW imaging system is based on solid-state electronic technology to radiate terahertz waves, and analyzes the internal structural features of objects by detecting the transmission or reflection of terahertz waves at different interfaces [20]. In the reflective real-aperture terahertz detection method, a set of optical lenses focuses the antenna radiation beam onto the focal plane (generally the surface of the sample under test), allowing for more concentrated energy, ultimately achieving tomographic imaging and three-dimensional (3D) reconstruction [2]. However, according to the principles of optical interference, terahertz waves have longer wavelengths and lower frequencies compared to infrared light and X-rays, resulting in slower phase variations. This implies that terahertz waves have longer coherence lengths. Therefore, in terms of spectral characteristics, using coherent light imaging undoubtedly impacts the longitudinal precision of terahertz detection [21].

In fact, many scholars and researchers have proposed various solutions to the issue of low longitudinal detection resolution in terahertz detection imaging. In terms of hardware, numerous researchers have put forward novel types of terahertz detectors, including high-sensitivity detectors, nano-detectors, and integrated detectors, to enhance the terahertz wave detection capability and resolution [22]. Wide-band terahertz sources have also been gradually proposed based on the theory that the coherence length of the radiation source is inversely proportional to the spectral width of the radiation source, but this approach causes dispersion issues [23]. Moreover, when altering the type of the sample under test and the optical path, it is necessary to adjust dispersion compensation devices, which seriously affects the detection efficiency. For linear FMCW radar imaging systems, Hu and Xu et al. have proposed combining multiple frequency bands to expand the bandwidth of the imaging system to improve the longitudinal resolution of detection, but undoubtedly this greatly increases the system complexity and detection cost [24]. In terms of signal processing methods, Hu et al. [25] proposed a high-precision distance-dimensional reconstruction algorithm. Initially, the MUSIC method is introduced to characterize high-resolution ranges and obtain the initial values of echoes, and then multiple Gaussian functions are used to fit and extract parameters from the echoes, allowing for a more precise and flexible reconstruction of distance profiles. However, this method still maintains relatively large errors in the detection results. In recent years, continuous wavelet transform (CWT) has been more and more widely used in the field of signal processing and data analysis. It can decompose signals into sub-signals of different scales and frequencies, providing the ability to analyze the local features of the signal. Dai and Zhou et al. [1,26] processed the detection signals of the measured sample using CWT and obtained wavelet coefficients that are more accurate than the original signals. However, this method is only effective for samples with the single structure, and its effectiveness is limited for the multi-layered samples with different materials. Additionally, the contrast of the reconstructed defects decreases, and for thinner specimens with more concentrated energy, it is more difficult to extract the interfacial features and defect features in multi-layered adhesive structures, such as aircraft TPS.

This paper evaluates the feasibility of using the continuous-wave terahertz detection system for contactless and NDT in multi-layered adhesive structures. Defect detection experiments were conducted on both multi-layered single-material adhesive structures and multi-layered different-material adhesive structures, confirming the applicability of terahertz FMCW technology as an advanced NDT tool for layered structures. A local adaptive empirical wavelet coefficient modal decomposition (LAEWCMD) method is proposed to realize the tomographic imaging and 3D reconstruction. Firstly, the region segmentation based on the two-dimensional (2D) terahertz images is conducted to divide the defects into different regions according to connectivity. Subsequently, CWT is applied to the range of the signals in each respective region to obtain continuous wavelet coefficients (CWCs). Then, empirical mode decomposition (EMD) is performed on the CWCs to extract the 1st intrinsic mode function (IMF) for 3D reconstruction. Finally, fusion is carried out. The effectiveness of the proposed method is verified on the aircraft TPS, and a more accurate 3D reconstruction is realized. This is instructive for terahertz FMCW technology in engineering applications.

2. Terahertz FMCW experimental test for NDT

2.1. Principle of FMCW radar detection

The experiments in the paper rely on a reflective terahertz FMCW detection platform, which consists of the terahertz radar, three linear actuators, a 2D scanning stage, a data acquisition unit and a human-machine interaction unit. The basic architecture of the terahertz detection system and the FMCW measurement principle are given in Fig. 1. The terahertz radar [27] used is manufactured by TRILITEC GmbH and the physical diagram is given by the red dashed box in Fig. 1(a). The radar operates from 126 GHz to 182 GHz and is connected to the data processing unit through a USB interface. The optical lenses used are made of polyethylene and are highly transmissive (see Fig. 1(b)). Lenses with a focal length of 50 mm are commonly used, concentrating energy within the depth of focus. Experimental verification shows the minimum detectable size range to be 2 mm. Figures 1(c) and (d) show the terahertz radar workflow and the FMCW measurement principle, respectively. The detecting time is determined by the size of the sample. During the actual detection, it takes about 0.2s to measure 1 unit area.

Initially, the ramp generator drives a voltage-controlled oscillator (VCO) to generate the fast saw tooth low-frequency sweep signal. Then the low-frequency sweep signal is multiplied by a frequency multiplier to become the transmitted signal (TX) of the terahertz system. A portion of the TX is radiated into the air by a horn antenna, while another portion serves as the reference signal directly entering the mixer. The TX radiated into the air converges at the focal plane by a focusing lens. When encountering interfaces of different media, it is reflected back to the terahertz source along the same path and then enters the mixer as the received signal (RX). The TX and RX are down-converted in the mixer, and the output intermediate frequency (IF) signal is ultimately recorded by an analog-to-digital converter (ADC).

Optics EXPRESS

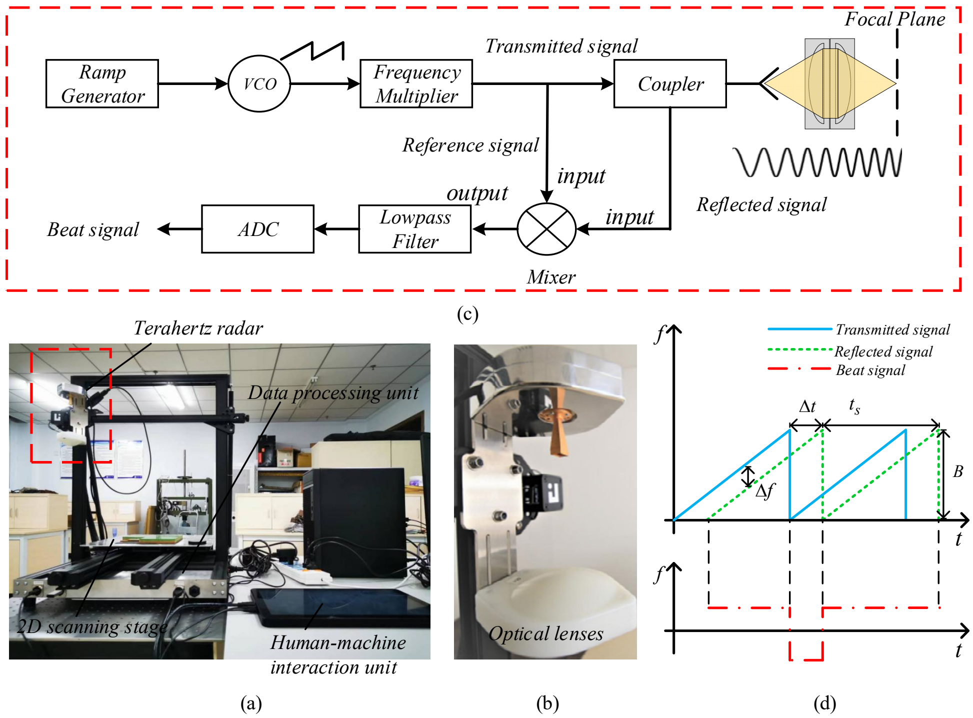

Fig. 1. Terahertz detection system architecture and measurement principle. (a) The physical diagram of the system. (b) Terahertz radar and optical lenses. (c) Terahertz radar workflow. (d) FMCW measurement principle.

The TX chirp and RX chirp can be expressed by the following equation:

$$S_{TX}(t) = A_t exp\left[j2\pi\left(f_0 t + \frac{1}{2}Kt^2\right)\right] \tag{1}$$

$$S_{RX}(t) = A_r exp\left\{j2\pi\left[f_0(t-\Delta t) + \frac{1}{2}K(t-\Delta t)^2\right]\right\} \tag{2}$$

where, A_t and A_r denote the amplitude of the emitted and reflected signals, respectively, f_0 is the initial frequency, K is the chirp rate and can be expressed by B/t_s, B is the system bandwidth, t_s is the sweep time, and Δt is the delay time.

When terahertz FMCW signals interact with layered structures during detection, different material layers correspond to different delay times, and the delay time gradually increases with the thickness of the material layer. The data obtained by terahertz radar is the sum of cosine functions at different frequencies, with each frequency component corresponding to different material interfaces.

The IF signal can be represented by the following formula:

$$S_{IF}(t) = \frac{A_t A_r}{2} exp\left[j2\pi(tK\Delta t) + f_0\Delta t - \frac{1}{2}K\Delta t^2\right] \tag{3}$$

After FFT transform, we can get the relationship between the differential beat frequency and the distance. The distance can be calculated as shown below:

$$d = \frac{ct_s\Delta f}{2nB} \tag{4}$$

where, c is the speed of light, n represents the refractive index of the material in the operating frequency band of the terahertz system. According to this detection principle, the sample can be scanned and detected point by point to obtain longitudinal information at each position of the sample, and ultimately, the 3D reconstruction of the sample interior can be realized.

2.2. Sample introduction

To evaluate the non-contact detection and transparent imaging capabilities of the terahertz FMCW system for layered structures, we conducted detection experiments in different scenarios using the single material bonding structure and multiple different material bonding structures.

In the single-layer structure detection (SSD) scenario, polyimide foam insulation is used as Sample 1, with dimensions of 90mm*90mm*30 mm, and six metal rings with an outer diameter of 10 mm and an inner diameter of 5 mm are prefabricated internally at different depth locations. Figure 2 shows the physical image and structural design schematic of Sample 1.

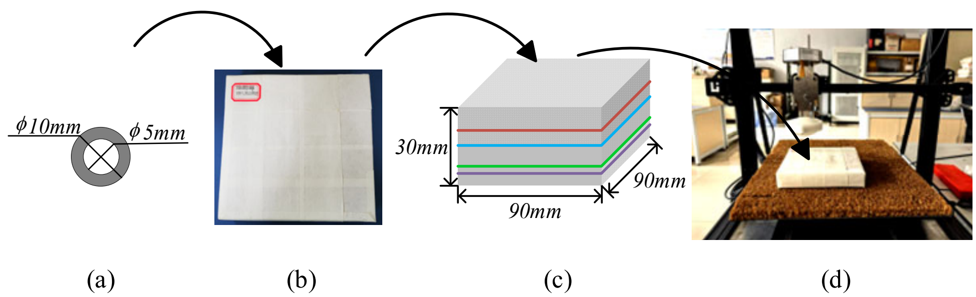

Fig. 2. Physical image and structural design schematic of Sample 1. (a) Defective structure. (b) Physical image. (c) Dimensional design schematic. (d) Scanning imaging scheme.

In the multi-layer structure detection (MSD) scenario, Sample 2 is made by CMC (35 mm), insulating felt (2 mm), and metal plate in sequence with epoxy resin adhesive (0.2 mm). And the dimensions are 180mm*135 mm, and two rows of defects are prefabricated in adhesive layer 1 and 2, respectively. Figure 3 shows the physical image and structural design schematic of Sample 2.

2.3. Detection results and problem analysis

Detection experiments are conducted using a reflective terahertz FMCW detection platform. The scan step is set to 1 mm, the sweep time is 1.024 us, and the sampling rate is 1 MHz. In order to ensure the accuracy of depth information, the upper surface of the specimen is placed at the focal plane of the detection system, and the full matrix sampling method is employed for scanning.

The inspection results in different depth directions for the two specimens are given in Fig. 4 and Fig. 5, respectively. For Sample 1, the image at the sampling point 1445 along the Z-axis represents the upper surface, the sampling point 1625 represents the lower surface, and the sampling point 1490 and 1535 represent typical internal positions. For Sample 2, the image at the sampling point 1682 represents the glue layer 1, the sampling point 1712 represents the glue layer 2, and the sampling point 1692 and 1702 represent typical internal positions.

Observing the imaging results of the two samples at different depths, it can be seen that the defects located on the lower surface of the laminate structure are recognized at the upper surface of the sample and at the internal location, especially in the MSD detection scenario. In other words, the terahertz wavelength is too long and the diffraction effect of the lens, which leads to a large pulse width of the reflected characteristic peaks, and the signal merging problem between the upper and lower surface signals of the laminated structure that are too close to each other (see Fig. 4(b) and Fig. 5(b)). This ultimately reduces the longitudinal resolution of the detection

Optics EXPRESS

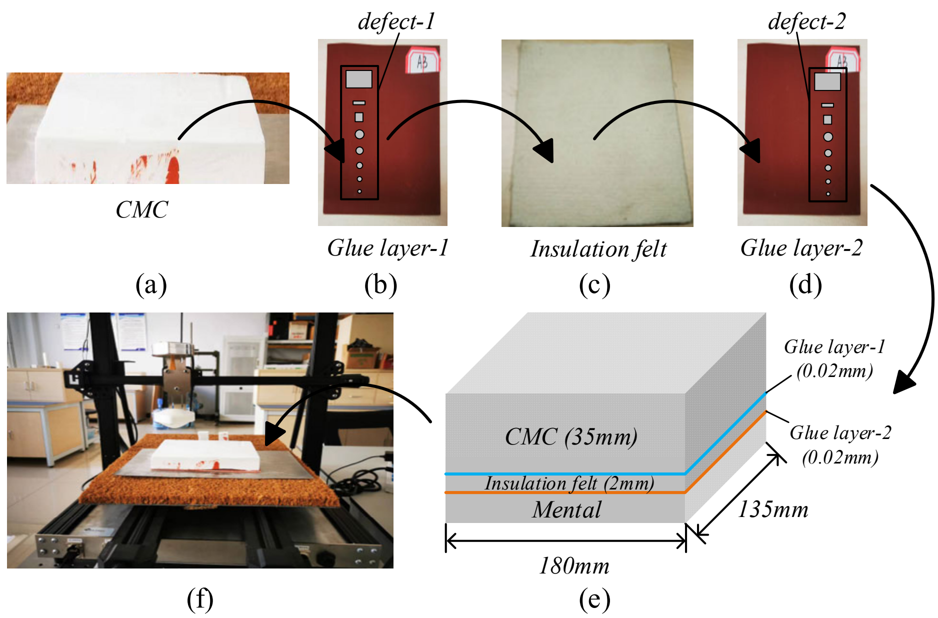

Fig. 3. Physical image and structural design schematic of Sample 2. (a) CMC (35 mm). (b) Glue layer-1 (0.02 mm), with a row of debonding defects. (c) Insulation felt (2 mm). (d) Glue layer-2 (0.02 mm), with a row of debonding defects. (e) Dimensional design schematic. (f) Scanning imaging scheme.

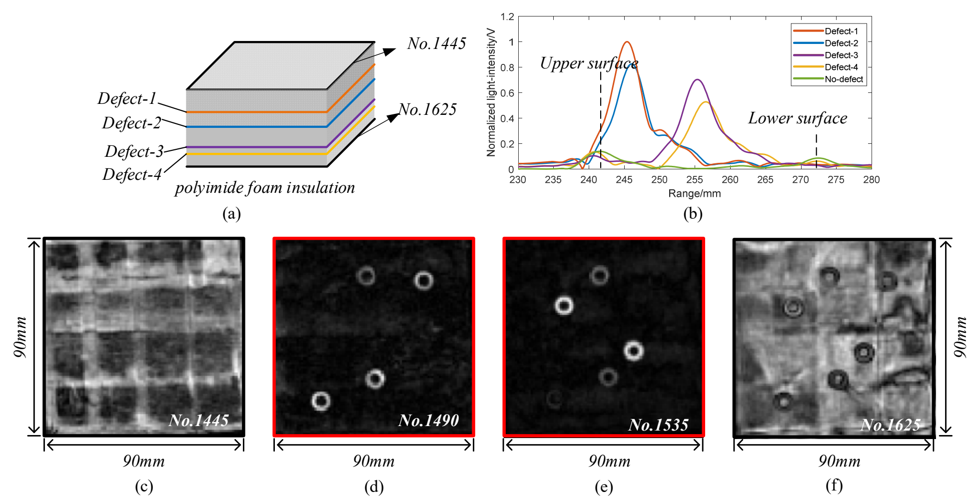

Fig. 4. The images at different sampling points along the Z-axis in Sample 1. (a) Dimensional design schematic. (b) Schematic of typical regional A-scan signals. (c) The sampling point 1445, corresponding to the upper surface of Sample 1. (d) The sampling point 1490. (e) The sampling point 1535. (f) The sampling point 1625, corresponding to the lower surface of Sample 1.

results and prevents an accurate judgment of the location of prefabricated defects. To overcome this problem, a local adaptive empirical wavelet coefficient modal decomposition method is proposed for tomography imaging and 3D reconstruction.

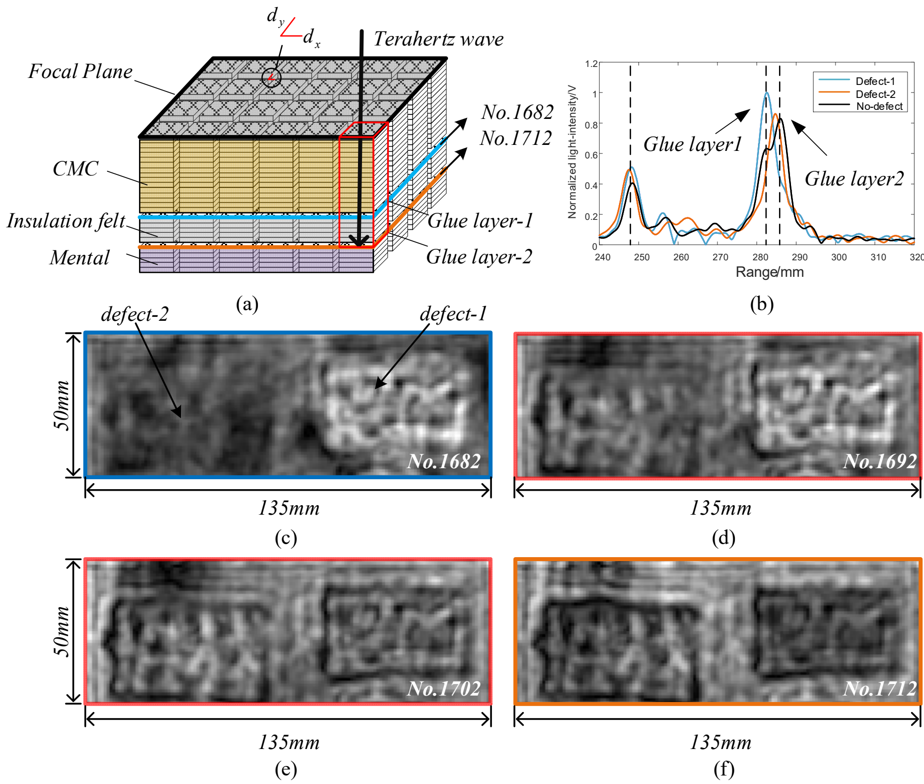

Fig. 5. The typical region images at different scan points along the Z-axis in Sample 2. (a) Dimensional design schematic. (b) Schematic of typical regional A-scan signals. (c) The scan point 1682, corresponding to glue layer 1. (d) The scan point 1692. (e) The scan point 1702. (f) The scan point 1712, corresponding to glue layer 2.

3. Method

3.1. Continuous wavelet transform

Wavelet transform refers to the decomposition of the original signal into various scales under the action of a set of wavelet basis functions. It allows for observing the overview of the signal in large-scale space and examining detailed information in small-scale space, thereby providing a better description of the signal's instantaneous characteristics. Different from the traditional Fast Fourier transforms (FFT), wavelet transforms have good local feature representation capabilities in both the time domain and frequency domain when analyzing non-periodic signals. Generally, in a square integrable space, the CWT of a continuous integrable function is defined as follows:

$$CWT(a,b) = \int_{-\infty}^{+\infty} x(t)\frac{1}{\sqrt{|a|}}\psi\left(\frac{t-b}{a}\right)dt \tag{5}$$

where $CWT(a,b)$ is the CWC, a and b are the scale factor and translation factor, respectively, and $\psi(t)$ is the wavelet basis function. The corresponding tolerance conditions should also be satisfied for the wavelet basis functions, which are represented by the following equation:

$$\int_{-\infty}^{+\infty} \frac{|\hat{\psi}(\omega)|^2}{|\omega|}d\omega<\infty \tag{6}$$

where $\hat{\psi}(t)$ is the FFT of $\psi(t)$. In the CWT, a determines the size of the wavelet window. A larger a leads to higher time resolution, which helps to better capture rapid changes in the signal and enhances the analysis capability in the time domain. When a is small, the width of the wavelet window increases, which improves the frequency resolution and can be used for the purpose of accurately extracting detailed information from the original signal.

3.2. Empirical wavelet coefficient mode decomposition

EMD is a commonly used signal processing method, particularly suitable for nonlinear and non-stationary signals. Unlike the FFT and CWT, EMD can decompose signals solely based on the scale characteristics of the signal, without being constrained by base functions. EMD can decompose the original signal into a series of IMFs and a residual function, where each IMF contains different timescale characteristics of the original signal and is relatively more stable than the original signal. Furthermore, each order of IMF needs to satisfy two conditions: on the one hand, the number of extreme points and the number of zero crossings are either equal or differ by at most one in all time scales; on the other hand, at any moment, the mean value of the envelope defined by the local maxima and local minima must be zero.

The EWCMD method refines the multiscale analysis based on CWT. Due to the reflection characteristic peaks of different heterogeneous medium interfaces contained in the range of terahertz signals, it is necessary to perform FFT on the terahertz echo time-domain signal to obtain its frequency domain information. Subsequently, the CWT is used to process the range of terahertz signals, decomposing the measured signal at various scales, analyzing low-frequency information in large-scale space, high-frequency information in small-scale space, and enhancing the interface features. Through experiments, it is found that the combination of wavelets using haar as the mother wavelet function and scale of 4 is able to maintain the signal characteristics well while suppressing the noise.

The signal processed by the EWCMD method is represented by the following equation:

$$W = \sum_{k=1}^{n} IMF_k(t) + r_n(t) \tag{7}$$

where $IMF_k(t)$ is the kth IMF component and $r_n(t)$ is the residual function. The decomposition process is as follows in Algorithm 1:

Algorithm 1. EWCMD

Step 1. Calculate the local maxima and local minima of the CWCs within the entire time range.

Step 2. Connect all local maxima to form the upper envelope line, connect all local minima to form the lower envelope line, and calculate the average of the upper and lower envelopes, denoted as $m_1(t)$.

Step 3. Extract the new data sequence $h_1(t) = W - m_1(t)$.

Step 4. Extract the local extreme points in $h_1(t)$, and repeat Step 2 ~ 4 until $h_1(t)$ satisfies the basic conditions of IMF. Record this data sequence as $IMF_1(t)$ and output it.

Step 5. Define a new signal represented as $r_1(t) = W - IMF_1(t)$, repeat steps 1 ~ 4 for $r_1(t)$, to obtain the remaining $IMF(t)$ and $r_n(t)$, until $r_n(t)$ becomes a monotonic function or a constant.

End

3.3. Improved adaptive threshold local ternary pattern method for 3D reconstruction

The 3D reconstruction is the process of using data obtained from multiple 2D images or scans to reconstruct the internal information of the measured object through specific algorithms and methods. However, in some cases, global reconstruction methods may not effectively reflect the local and spatial features of the images, especially in low SNR detection scenario, where the reconstruction results are significantly affected by noise. Therefore, Local Binary Pattern (LBP) is prone to losing texture features and cannot accurately describe image details. In this paper, an improved adaptive threshold local ternary pattern (ATLTP) method is introduced for 3D reconstruction based on the EWCMD method. This method first globally normalizes the values on each range, then performs adaptive threshold segmentation on each value according to the grayscale difference of the neighborhood, and finally merges the results.

Figure 6 illustrates a 3*3*3 3D pixel space region. The gray value of the central pixel is defined as g_0, and the gray value of the neighboring pixels is $g_i(i = 1, 2, \cdots, 26)$. The average of the neighboring pixel values and the central pixel can be represented by the following equation:

$$g_a = \frac{1}{P+1}\sum_{i=0}^{P} g_i \tag{8}$$

where P is the preset number of pixel fields. Then the difference between the pixels and the mean value of each field and the mean value of the difference can be calculated by the following equations:

$$\Delta g_a = g_i - g_a \tag{9}$$

$$\overline{\Delta g_a} = \frac{1}{P}\left(\sum\nolimits_{i=0}^{P-1} |\Delta g_a|\right) \tag{10}$$

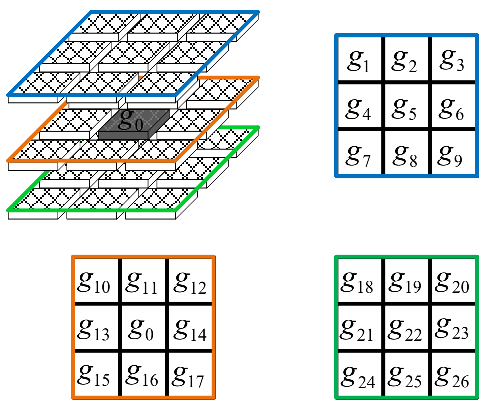

Fig. 6. A 3*3*3 3D pixel space region.

Define the adaptive threshold range as $[c - k\alpha, c + k\alpha]$, where c is the grayscale value of the central pixel, k is the weighting coefficient. The improved LTP method can be represented by the following equation:

$$S(g_i, g_c, k, \alpha) = \begin{cases} 1, & g_i > g_c + k\alpha \\ 0, & |g_i - g_c| \le k\alpha \\ -1 & g_i < g_c - k\alpha \end{cases} \tag{11}$$

Compared with the traditional LTP algorithm, the improved ATLTP algorithm can preserve the relative relationship between the central pixel and its neighborhood, while reducing the dependence on the central pixel. In addition, based on the calculation of the neighborhood pixel discretization, a weight coefficient k is introduced, which makes the threshold for extracting defect features at different levels more precise and beneficial for 3D reconstruction. At the same time, the size of the threshold will also change with the change of local pixels, achieving adaptability of the threshold.

4. Experiments

In the experiments, Gaussian, Daubechies, Symlet, Coiflet and Haar wavelets were used for comparison. The Haar2 wavelet mother function was chosen for the next experiment with the best reconstruction results.

4.1. SSD scene detection experiment

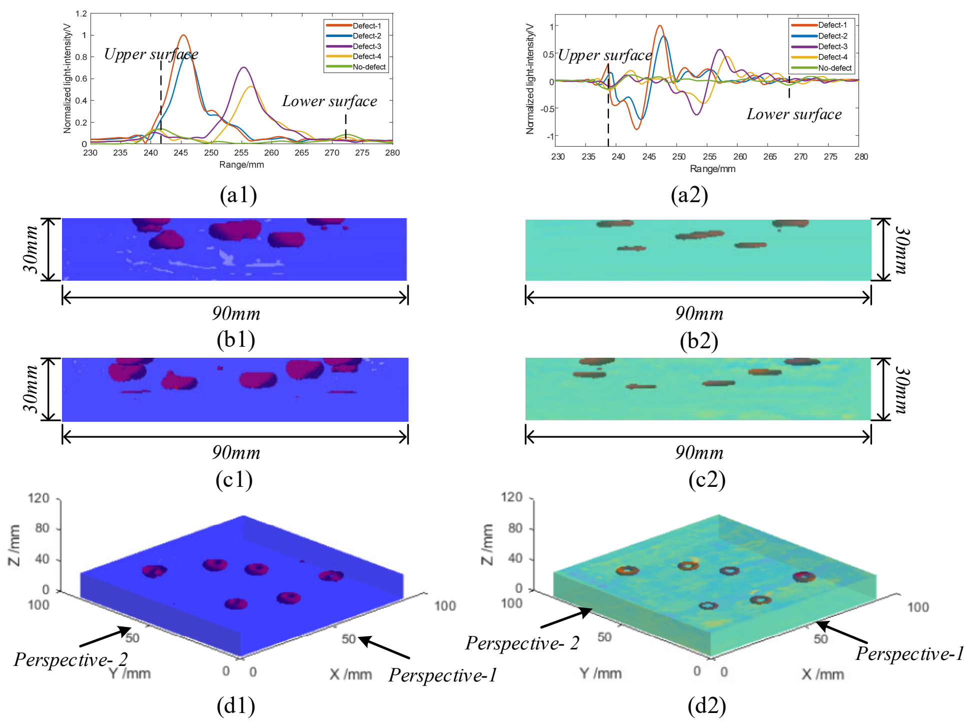

Fig. 7. Comparison of detection results in SSD scenarios (Sample 1). (a1~a2) The comparison of results before and after processing for five typical signals, including four typical signals at the defects with different depths and one signal at the no-defects. (b1~b2) The B-scan images at perspective 1. (c1~c2) The B-scan images at perspective 2. (d1~d2) The 3D reconstruction results before and after processing.

In the SSD detection experiment, the proposed LAEWCMD method is applied to the detection signals, and the reconstructed results are obtained as shown in Fig. 7. Here, (a1~a2) respectively illustrate the comparison of results before and after processing for five typical signals, including four typical signals at the defects with different depths and one signal at the no-defects. (b1~b2) and (c1~c2) are the B-scan images at perspective 1 and perspective 2, respectively. (d1~d2) are the 3D reconstruction results before and after processing. Influenced by different material interfaces, the terahertz wave contains multi-level reflection characteristic peaks reflecting different depth positions in the range, and due to the attenuation characteristics during propagation in the material, the energy of the reflection peaks gradually weakens. What's more, the diffraction effect of terahertz waves and lenses leads to a large pulse width of the reflection feature peaks, and the reconstruction results show an expansive nature, which strips the original appearance of the specimen (e.g., Fig. 7(b1~d1)). With the effect of the algorithm proposed in this paper, the local differences between defect reflection signals at different depths are enhanced, making the signals more compact and the reconstructed results closer to the real situation.

4.2. MSD scene detection experiment

In the MSD detection experiment, the loose and porous nature of CMC leads to a certain absorption of terahertz waves. Additionally, the nonlinear cliff attenuation of terahertz waves in free space implies that as the detection depth increases, the detection becomes more challenging and the reconstruction results deteriorate [5].

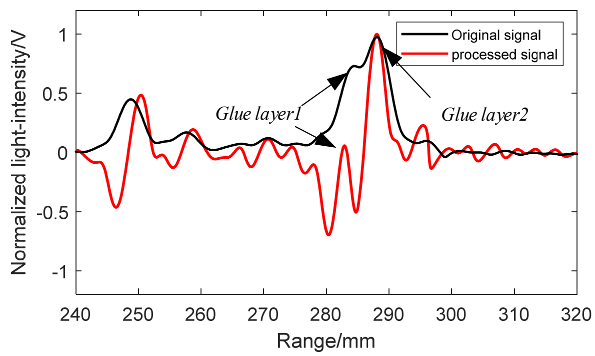

Fig. 8. Typical signal representations before and after processing (Sample 2).

The proposed LAEWCMD method is applied to the range of one-dimensional terahertz detection signals. Typical signal representations before and after processing are illustrated in Fig. 8. The solid black line represents the original signal in the range dimension, while the red signal depicts the result after application of the proposed method. Due to the influence of different medium interfaces, terahertz waves in the range dimension exhibit multi-level reflection characteristic peaks reflecting various depths. Additionally, due to attenuation characteristics during propagation through the medium, the energy of these reflection peaks gradually diminishes. However, at the bottom of glue layer 2, which interfaces with a metal plate, total reflection occurs when encountering terahertz waves. Therefore, for no-defect positions in the range representation (black line), the peaks of glue layer 2 are higher than those of glue layer 1.

Due to the diffraction effects of terahertz waves and the lens, the pulse width of reflection characteristic peaks is large, significantly affecting the layering accuracy. The algorithm proposed in this paper enhances the local variability between defect reflection signals at different depths, resulting in a more compact signal representation and processing results that are closer to reality. Figure 9 illustrates the schematic of sample detection slices. The detection challenges of TPS originate from two aspects. Firstly, the low energy of terahertz echo signals at the adhesive layer, compounded by the irregularity of the bonding interface, significantly impacts imaging quality. Secondly, due to the longer wavelength of terahertz wave, closely spaced interfaces can produce signal "coalescence peaks", reducing the longitudinal resolution of the detection image and complicating defect localization. Defects in different bonding layers exhibit low energy reflection along a specific direction due to closed-loop characteristics and absolute scattering effects, aiding in enhancing differential features.

With the method proposed in this paper, the defective edge features of glue layer 1 and 2 can be clearly separated. The B-scan detection results under FFT, FFT-CWT, FFT-EMD, ECWCMD and LAEWCMD methods are given in Fig. 10. Among them, Figs. 10(a1~a5) show the B-scan images without defects, and it can be seen that the signals processed by FFT can provide range information. However, the long terahertz wavelength leads to the low longitudinal resolution,

Optics EXPRESS

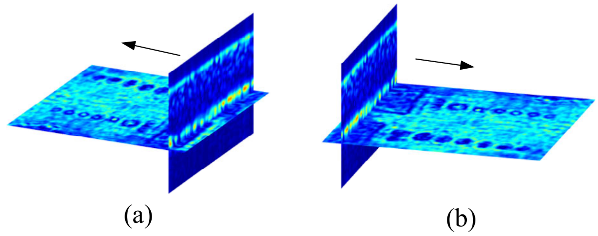

Fig. 9. The schematic of Sample 2 detection slices.

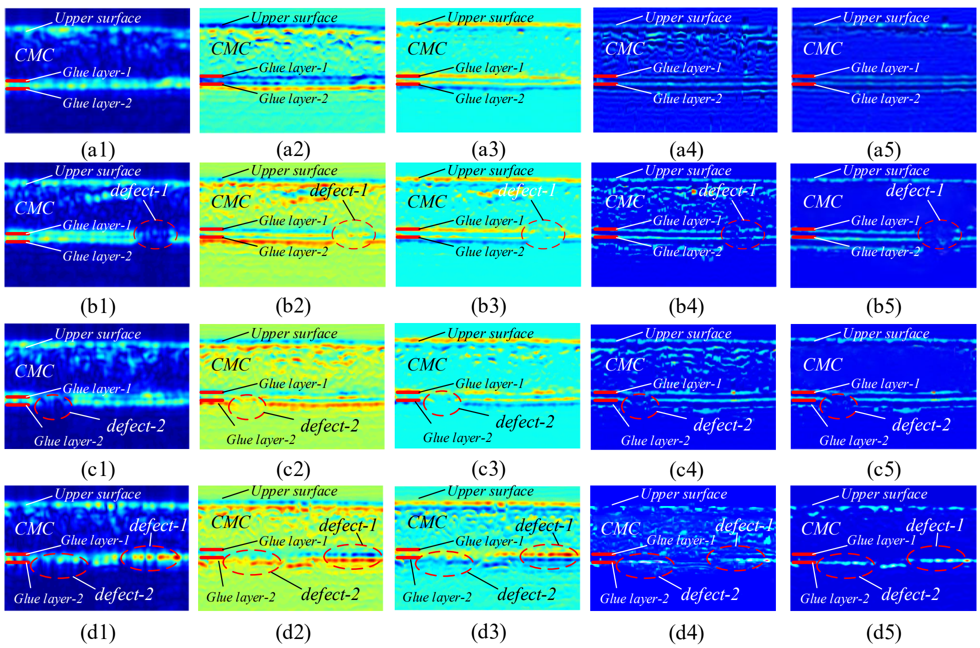

Fig. 10. The B-scan images of using FFT, FFT-CWT, FFT-EMD, ECWCMD, and LAEWCMD methods. (a1~d1) The B-scan images using FFT, with no defect, defect 1 edge, defect 2 edge, defect 1 and defect 2 position. (a2~d2) Results by FFT-CWT. (a3~d3) Results by FFT-EMD. (a4~d4) Results by ECWCMD. (a5~d5) Results by proposed LAEWCMD.

and the characteristic peaks of glue layer 1 and 2 are not easy to be distinguished. Through the processing with CWT, EMD, and their combined algorithms, the characteristics of glue layers 1 and 2 gradually become apparent. Finally, with the LAEWCMD method, the clutter is effectively filtered, enabling a clear distinction between glue layer 1 and 2. Figures 10(b1~b5) show the B-scan images at the edge of defect 1, where the low energy reflection at the defect edge causes scattering of the interface feature peaks of glue layer 1, resulting in no echo signals for either glue layer 1 or 2. Figures 10(c1~c5) display the B-scan images at the edge of defect 2, showing that the interface feature peak of glue layer 2 is scattered, while the interface feature of glue layer 1 can be distinctly identified. Figures 10(d1~d5) illustrate B-scan images at the positions of defect 1 and 2, where the debonding causes an increase in the peak values of the interface echo signals for glue layer 1 and 2. The method proposed in this paper enables a clear distinction of the characteristic peaks at different layers.

The 3D reconstruction results obtained by the proposed algorithm are given in Fig. 11, where (a) and (b) respectively show the overall and local reconstruction results, and (c) displays the

Optics EXPRESS

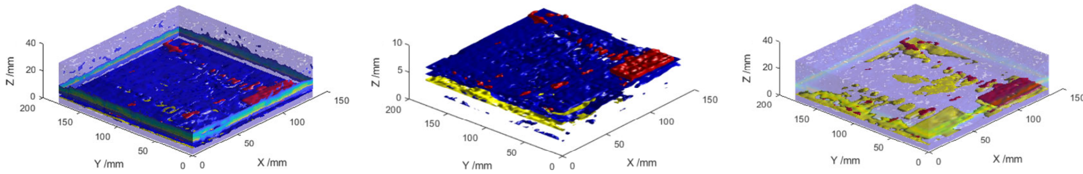

(a) (b) (c)

Fig. 11. The 3D reconstruction results of Sample 2. (a) Schematic of the overall reconstruction. (b) Schematic of the local reconstruction. (c) Schematic of the defect reconstruction, where the red part indicates defect 1 and the yellow part indicates defect 2.

defect reconstruction effect, with the red part indicating the defect 1 and the yellow part indicating the defect 2. It validates the effectiveness of the method proposed in this paper for the 3D reconstruction of TPS detection.

5. Conclusion

The inspection capabilities of the continuous-wave terahertz detection system are evaluated on polyimide foam insulation and aircraft TPS. It confirmed the applicability of terahertz FMCW technology for NDT of composite materials. A novel LAEWCMD method is proposed in this paper to overcome the low longitudinal resolution issue in terahertz detection caused by the long wavelength. Two sets of experiments SSD and MSD detection scenarios are designed, both of which validated the effectiveness of the proposed method to solve the problem of signal peak merging, so that the peak-phase merged echo signals are better separated. Additionally, the method effectively enhances the interface characteristic peaks while suppressing the noise when performing 3D reconstruction. These findings offer new insights and methods for the application of terahertz tomography imaging and 3D reconstruction.

Funding. National Natural Science Foundation of China (U23A20636); Natural Science Foundation of Shanxi Province (20210302124189, 202203021221118, 202302020101008); Shanxi Returned Scholarship Council (2022-145).

Disclosures. The authors declare no conflicts of interest.

Data availability. Data underlying the results presented in this paper are not publicly available at this time but may be obtained from the authors upon reasonable request.

References

1. B. Dai, P. Wang, T.-Y. Wang, *et al.*, "Improved terahertz nondestructive detection of debonds locating in layered structures based on wavelet transform," Compos. Struct. **168**, 562–568 (2017).
2. K.-L. Xue, W.-N. Zhang, Z.-B. Wang, *et al.*, "Real aperture continuous terahertz imaging system and spectral refinement method," Photonics. **10**(9), 1020 (2023).
3. K. Tomkiewicz, A. Plqskowski, M.-S. Beck, *et al.*, "Testing of the failure of a solid rocket propellant with tomography methods," Chem. Eng. J **77**(1-2), 73–78 (2000).
4. S. P. Song and Y.-J. Ni, "Ultrasound imaging of pipeline crack based on composite transducer array," Chin. J. Mech. Eng. **31**(1), 81 (2018).
5. K.-L. Xue, Y.-X. Chen, W.-N. Zhang, *et al.*, "Continuous terahertz wave imaging for debonding detection and visualization analysis in layered structures," IEEE Access. **11**, 31607–31618 (2023).
6. D.-H. Han, "Inner defect detection of glass fiber reinforced polymer sandwich panel using pulsed terahertz imaging based on smoothing and derivative," NDT&E Int. **138**, 102862 (2023).
7. J. Wang, T. Xu, L. Zhang, *et al.*, "Nondestructive damage evaluation of composites based on terahertz and X-ray image fusion," NDT&E Int. **127**, 102616 (2022).
8. J.-B. Perraud, J.-P. Guillet, O. Redon, *et al.*, "Shape-from-focus for real-time terahertz 3D imaging," Opt. Lett. **44**(3), 483–486 (2019).
9. C. Stoik, M. Bohn, and J. Blackshire, "Nondestructive evaluation of aircraft composites using transmissive terahertz time domain spectroscopy," Opt. Express **16**(21), 17039–17051 (2008).
10. J. Gao, Y. Qin, B. Deng, *et al.*, "A novel method for 3-D millimeter-wave holographic reconstruction based on frequency interferometry techniques," IEEE Trans. Microwave Theory Techn. **66**(3), 1579–1596 (2018).

Optics EXPRESS

11. H. Huang, P. Qiu, S. Panezai, *et al.*, "Continuous-wave terahertz high-resolution imaging via synthetic hologram extrapolation method using pyroelectric detector," Opt. Laser Technol. **120**, 105683 (2019).
12. W. Nsengiyumva, S. Zhong, B. Wang, *et al.*, "Terahertz spectroscopic study of optical and dielectric properties of typical electrical insulation materials," Opt Mater. **123**, 111837 (2022).
13. X. Zhang, Q. Guo, T. Chang, *et al.*, "Broadband stepped-frequency modulated continuous terahertz wave tomography for nondestructive inspection of polymer materials," Polym Test. **76**, 455–463 (2019).
14. J. Ren, L. Li, D. Zhang, *et al.*, "Study on intelligent recognition detection technology of debond defects for ceramic matrix composites based on terahertz time domain spectroscopy," Appl. Opt. **55**(26), 7204–7211 (2016).
15. X. Zhang, T. Chang, Z. Wang, *et al.*, "Three-dimensional terahertz continuous wave imaging radar for nondestructive testing," IEEE Access. **8**, 144259 (2020).
16. K.-B. Cooper, R.-J. Dengler, N. Llombart, *et al.*, "THz imaging radar for standoff personnel screening," IEEE Trans. Terahertz Sci. Technol. **1**(1), 169–182 (2011).
17. J.-F. Federici, B. Schulkin, F. Huang, *et al.*, "THz imaging and sensing for security applications—explosives, weapons and drugs," Semicond. Sci. Technol. **20**(7), S266–S280 (2005).
18. J.-P Guillet, M Roux, K Wang, *et al.*, "Art painting diagnostic before restoration with terahertz and millimeter waves," J. Infrared, Millimeter, Terahertz Waves **38**(4), 369–379 (2017).
19. Q. Cassar, A. Al-Ibadi, L. Mavarani, *et al.*, "Pilot study of freshly excised breast tissue response in the 300–600 GHz range," Biomed. Opt. Express **9**(7), 2930–2942 (2018).
20. M. Pauli, B. Gottel, S. Scherr, *et al.*, "Miniaturized millimeter-wave radar sensor for high-accuracy applications," IEEE Trans. Microwave Theory Techn. **65**(5), 1707–1715 (2017).
21. H. Essen, A. Wahlen, R. Sommer, *et al.*, "Very high bandwidth millimetre-wave radar," Electron. Lett. **41**(22), 1247–1249 (2005).
22. C. L. K. Dandolo, J.-P. Guillet, X. Ma, *et al.*, "Terahertz frequency modulated continuous wave imaging advanced data processing for art painting analysis," Opt. Express **26**(5), 5358–5367 (2018).
23. N. Schreiner, W. Sauer-Greff, R. Urbansky, *et al.*, "Multilayer thickness measurements below the Rayleigh limit using FMCW millimeter and terahertz waves," Sensors. **19**(18), 3910–3912 (2019).
24. W. Hu, Z. Xu, H. Jiang, *et al.*, "High range resolution wideband terahertz FMCW radar with a large depth of field," Appl. Opt. **61**(24), 7189–7196 (2022).
25. W. Hu, Y. Li, Z. Han, *et al.*, "High-resolution range profile reconstruction method for terahertz FMCW radar," Appl. Opt. **60**(22), 6400–6408 (2021).
26. Y. Zhou, T. Wang, B. Dai, *et al.*, "High-precision terahertz frequency modulated continuous wave imaging method using continuous wavelet transform," Opt. Eng. **57**(02), 1 (2018).
27. S. Kueppers, T. Jaeschke, N. Pohl, *et al.*, "Versatile 126–182 GHz UWB D-band FMCW radar for industrial and scientific applications," IEEE Sens. Lett. **6**(1), 1–4 (2022).